DOI: https://doi.org/10.15276/aait.09.2026.40
UDC 004.9

Two-channel shaft synchronization of a rotary vane engine with constrained electric drives

Yurii O. Ushenko[1)]
ORCID: https://orcid.org/0000-0003-1767-1882; y.ushenko@chnu.edu.ua. Scopus Author ID: 6701840218
Dmytro I. Uhryn[1)]
ORCID: https://orcid.org/0000-0003-4858-4511; d.ugryn@chnu.edu.ua. Scopus Author ID: 57163746300
Yurii O. Halin[1)]
ORCID: https://orcid.org/0009-0006-9629-9896; halin.yurii@chnu.edu.ua
[2)] Yuriy Fedkovych Chernivtsi National University, 2, Kotsyubynsky Str. Chernivtsi, 58002, Ukraine

ABSTRACT

Electromagnetic synchronization of rotary vane engine shafts requires coordinating the vane motion with a variable gas load within the limited capabilities of electric drives. The aim of the study is to develop a coupled computer model of shaft synchronization that accounts for mechanical and thermodynamic processes and the electrical limitations of permanent magnet synchronous drives with field-oriented control. The objectives are to formulate coupled equations of the shafts, chambers and drives, to develop a two-channel synchronization algorithm, to implement a reproducible simulator and to determine how drive parameters, chamber scale and gas leakage affect the stability of motion. The model combines two-shaft dynamics, chamber gas processes with heat release and seal leakage, and drives with current and voltage limits, winding inductance and resistance, proportional-integral current control, back electromotive force compensation, anti-windup protection, digital control and finite current-loop bandwidth. It is checked against analytical solutions, energy balances, the ideal Otto cycle and independent implementations of individual blocks. A two-channel algorithm is proposed that adaptively controls the relative motion of the shafts and corrects the position of the vane bisector relative to the housing; its local stability conditions are established. The influence of the physical torque reversal and gas leakage on the operability of synchronization is determined. The simulator allows electric machines, controller settings and engine geometry to be assessed before an experimental test bench is built. In the studied regimes the algorithm keeps a small steady-state bisector offset and restores synchronized motion after a misfire and changes in heat release and load. This is also confirmed by numerical tests with random initial conditions and varied electrical parameters of the studied drives. For the selected drive, the admissible chamber volume with combustion is bounded by the current from above and by leakage from below. Synchronization stability is determined by the torque reserve and the rate of torque build-up; current and voltage margins are necessary but not sufficient. Without combustion, the drive suffices for all studied volumes, so this mode suits initial bench tests. The quantitative results are model predictions requiring experimental confirmation.

Keywords: computer simulation; rotary-vane engine; shaft synchronization; field-oriented control; synchronous motor; seal leakage

For citation: **Ushenko Yu. O., Uhryn D. I., Halin Yu. O. "Two-channel shaft synchronization of a rotary vane engine with constrained electric drives". *Applied Aspects of Information Technology.* 2026; Vol.9 No.4: 615–631. DOI: https://doi.org/10.15276/aait.09.2026.40**

INTRODUCTION

Rotary vane internal combustion engines, also known as "cat-and-mouse" or opposed rotary piston engines, are electromechanical positive-displacement systems in which the working cycle is determined by the relative angular motion of two shafts equipped with vanes [1, 2]. The shafts rotate in the same direction with the same average speed, but with a periodic phase shift between them that forms the variable volume of the working chambers and implements the thermodynamic cycle without a crank mechanism [3].

The geometry of the chambers, the timing of the processes and the stability of operation depend directly on the accuracy of shaft synchronization. The principle of electromagnetic vane coordination, which replaces the mechanical gear train by flexible control of the phase shift, is described in the patent [4].

In computer models of such engines, synchronization is usually treated as a problem of mechanical coordination of motion implemented by control torques applied to the shafts. The electric machines are then represented as ideal torque sources without their own dynamics. In the previous work [5] such an idealized model was developed; it demonstrated the fundamental feasibility of electromagnetic phase control, but did not take into

© Ushenko Y., Uhryn D., Halin Y., 2026

This is an open access article under the CC BY license (https://creativecommons.org/licenses/by/4.0/deed.uk)

account the physical limitations of the motors. The conference paper [6] added a current-loop model of a permanent magnet synchronous motor (PMSM), but kept two idealizations: the sign of the drive torque was reversed in the mechanical equations at the end of each stroke, which corresponds to an instantaneous reversal of the current, and gas leakage was described by a constant coefficient.

A real PMSM drive has limitations that cannot be ignored. The winding current is limited by thermal stability and power electronics, which bounds the available torque; the back electromotive force (back-EMF) grows with speed and reduces the voltage margin for forcing the current; and the bandwidth of the current loop, the rate at which the controller can track the torque command, is finite. In addition, increasing the torque constant K_t gives more torque per ampere but also increases the back-EMF and reduces the voltage margin. Leakage of gas through the seal gaps, which shapes the gas torque, has not yet been integrated into coupled electromechanical models of rotary vane engines, although the disturbing torque changes sign within every stroke and is not typical of conventional field-oriented control (FOC) problems.

The purpose of this work is to eliminate the idealizations of the models [5, 6] and to develop a coupled model of a rotary vane engine with a physically constrained electric drive under field-oriented control, which accounts for current and voltage limitations, the current-loop dynamics with PI controllers, back-EMF compensation, anti-windup and pressure-dependent leakage, and to check whether the adaptive synchronization algorithm remains operable under these constraints.

ANALYSIS OF LITERATURE DATA

Gao et al. [1] investigated the design of a small-scale opposed rotary piston engine of this type without crank connecting rods and valves and estimated its fuel consumption and power density by one- and three-dimensional simulation. Wang et al. [2] developed a mathematical model of the kinematics of such an engine with an elliptical gear pair and related the piston motion, the chamber volume and the compression ratio to the gear eccentricity. Heywood [3] summarized the zero-dimensional cycle theory that forms the basis of such models. Later works refined the chamber processes by two-zone simulation of an axial vane rotary engine [7], CFD analysis of flow and combustion [8], rotary valves [9], high-speed rotary designs [10] and the efficiency of rotary thermal systems [11]. Leakage past the seals is the main loss mechanism of rotary engines: it depends on the pressure ratio and gap geometry [12] and strongly affects the cycle [13]. None of these works considers the limitations of the electric drive as a factor of synchronization.

In the first paper of this series [5], an adaptive synchronization algorithm was developed that corrects the drive torque after every stroke from the bisector offset of the vanes and the change of their kinetic energy. It reduced the bisector offset to thousandths of a degree, but used an idealized torque source. The conference paper [6] introduced a current-loop model and estimated the admissible engine scale from the torque reserve of the drive.

The theory of AC drive control is based on the d–q model of the PMSM by Pillay and Krishnan [14] and on field-oriented control with cascaded PI current loops, back-EMF compensation and anti-windup described by Boldea and Nasar [15] and Sul [16]. The ODrive documentation [17] gives the constants of laboratory PMSMs in phase-amplitude units. When the load is periodic and fast compared with the sampling period, the computation delay and the low ratio of sampling to fundamental frequency degrade current control [18]. These sources consider quasi-stationary or slowly varying loads; the case of a gas torque that reverses every few milliseconds remains outside the scope of the existing FOC studies.

Synchronization of several axes has been investigated in related fields. Havrylenko and Kulinich [19] studied the synchronization of hydraulic motors and showed the role of inertial effects. Wang, Chen and Zhang [20] proposed adaptive cross-coupled control for multi-axis systems, and the reviews [21, 22] systematize master–slave, virtual-shaft and deviation-coupling structures. The closest dynamic analogue is the free-piston engine generator, in which the dead centres are stabilized by the electric machine [23], whose load and motion profile shape the cycle [24, 25]. Digital twins of machines and drives are used to select hardware before prototyping [26]. None of these approaches is adapted to two rotors coupled only through the gas.

Thus there is a gap at the intersection of three areas: studies of rotary vane engines do not account for the dynamic limitations of drives; FOC studies do not consider rapidly reversing gas loads; and multi-axis synchronization methods are not adapted to the gas coupling of the rotors. The trade-off of the torque constant and the influence of leakage through the seals on the disturbing torque have not been studied in coupled electromechanical models, and

neither [5] nor [6] gives a formal criterion of stable synchronization or stability conditions of the algorithm.

PROBLEM STATEMENT

Accurate synchronization of rotary vane engine shafts requires the drives to compensate for a rapidly varying gas torque. Existing models represent the electric machines as ideal torque sources, whereas in a real PMSM drive the torque is limited by the winding current, resistance and inductance, back-EMF and the finite bandwidth of the current loop. Thus, a motor with sufficient nominal torque may still be unable to keep the shafts synchronous. A physically constrained electromechanical model is therefore required to determine, with a formal criterion, the conditions under which synchronization remains stable and to select the engine geometry, motor parameters and power electronics.

AIM AND OBJECTIVES OF THE STUDY

The purpose of the study is to develop and substantiate a coupled computer model of shaft synchronization of a rotary vane internal combustion engine that takes into account the mechanics of the shafts, the gas torque in the working chambers, gas leakage and the physical limitations of PMSM drives with field-oriented control.

The practical goal is a simulation tool for the preliminary evaluation of drive configurations and engine parameters before a laboratory test bench is built: the admissible working-chamber scale, the proximity to current and voltage limits and the influence of the drive and gas-cycle parameters on synchronization stability.

To achieve this goal, the following tasks were set:

1) to analyse the existing approaches to rotary vane engine synchronization, field-oriented drive control and multi-axis coordination;

2) to develop a coupled model of the two-shaft mechanics, the gas torque in the working chambers and the gas leakage through the seal gaps;

3) to develop a physically constrained model of the PMSM drive with field-oriented control, current and voltage limitations, anti-windup and finite current-loop bandwidth;

4) to integrate the drive model with the adaptive synchronization algorithm, to refine the algorithm where the physical model requires it and to implement a computer simulator for the numerical analysis of shaft motion, bisector offset, stroke duration, motor current and inverter voltage;

5) to determine the admissible working-chamber scale and the stability of synchronization in the baseline mode simulating butane combustion;

6) to investigate the influence of gas leakage and of the working medium on the peak drive load and synchronization stability;

7) to determine the range of applicability of the model as a tool for the preliminary screening of drive configurations.

MATERIALS AND RESEARCH METHODS

This study uses a computer model of the shaft synchronization system of a rotary vane engine with two electric drives, which checks whether the vanes remain synchronous under the real physical limitations of electric motors and power electronics. Unlike the idealized model [5], the desired torque is first converted into a current command, and the actual torque appears only after the current loop of the field-oriented drive. The model consists of five blocks (Fig. 1): the synchronization algorithm, the two drives with four PI current controllers (d and q axes of each motor), the mechanics of the two shafts, the working chambers and the block of event measurements, which uses only the encoder signals.

Selection of the scaled engine size

The geometry of the original patent solution corresponds to an engine with a much larger working volume, whose gas torque exceeds the capabilities of a compact laboratory drive. The geometry was therefore scaled down to verify the synchronization concept itself. The working-sector volume V_s of one chamber (the parameter “chamber volume” of the simulator) defines all dimensions: with the dead-zone (vane) angle U_L = 40°, the sector $\varphi_s = \pi - 2U_L$, the adopted proportions $R_2 = 3R_1$, $h = 2R_1$ and the compression ratio ε = 9,

$$R_1 = \frac{1}{2}\left(\frac{V_s}{\varphi_s}\right)^{1/3}, \quad \frac{dV}{d\alpha} = \frac{h\left(R_2^2 - R_1^2\right)}{2} = 8R_1^3, \quad u_1 = \frac{\varphi_s}{\varepsilon+1}, \quad u_2 = \frac{\varepsilon\varphi_s}{\varepsilon+1}, \tag{1}$$

where R_1, R_2 are the inner rotor and housing radii, h the axial width and u_1, u_2 the chamber angles at the dead centres; the chamber volumes are $V_x = x\,dV/d\alpha$ and $V_c = (\varphi_s - x)\,dV/d\alpha$, where x is the relative angle of the expansion chamber.

The moment of inertia of a shaft with two vanes (steel density ρ) and an added flywheel J_f is

$$J = 320\,\rho\,U_L R_1^5 + J_f. \tag{2}$$

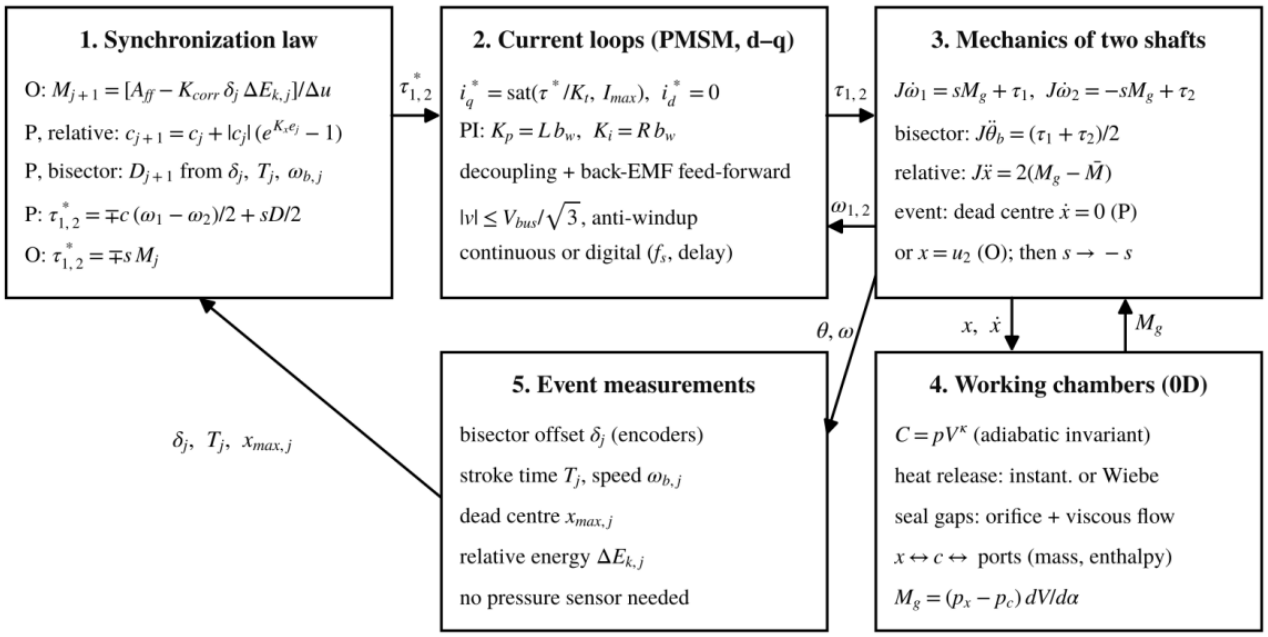


Fig. 1. **Structure of the computer model and of the control system: synchronization algorithm (block 1), current loops of the two drives (block 2), shaft mechanics (block 3), working chambers (block 4) and event measurements (block 5)**

***Source*: compiled by the authors**

For the baseline volume of 4.0 cm³ the housing diameter is about 40 mm, and 82 % of the inertia is the flywheel. The volume enters the model through (1) and (2): the gas torque grows as V_s, the inertia as $V_s^{5/3}$ and the seal perimeter only as $V_s^{1/3}$.

Gas cycle and leakage modeling

The gas cycle describes the pressure in the compression and expansion chambers. In the earlier model [6], leakage was taken into account by reducing the temperature rise after combustion, $\Delta T_{eff} = \Delta T(1 - \lambda)$; this lumped coefficient λ is kept only as an option for comparison. In the present model each active chamber is a single-zone ideal gas with mass m, pressure p and temperature $T = pV/(mR_g)$, and the solver integrates the adiabatic invariant $C = pV^{\kappa}$, which is exactly constant in a closed chamber without heat release:

$$\frac{dC}{dt} = V^{\kappa-1}\left[(\kappa-1)(\dot{Q} - \dot{Q}_w) + \kappa R_g \textstyle\sum_k \dot{m}_k T_k\right], \quad \frac{dm}{dt} = \textstyle\sum_k \dot{m}_k, \quad p = \frac{C}{V^{\kappa}}, \tag{3}$$

where κ = 1.3 is the constant ratio of specific heats adopted for the mixture of air and combustion products [3], $\dot{Q}$ is the heat-release rate, $\dot{Q}_w$ the wall heat flux (zero in the baseline, i.e. adiabatic walls), $\dot{m}_k$ are the mass flows through the seal gaps and T_k their upstream temperatures. In the baseline mode the temperature rise after combustion is ΔT = 2200 K, which corresponds to a stoichiometric butane–air mixture; the heat $Q = mc_v\Delta T$ is released at the dead centre either instantaneously or by the Wiebe law

$$x_b = 1 - \exp\left[-a_W\,\zeta^{m_W+1}\right], \quad \zeta = \frac{x - x_{ig}}{\Delta\varphi_b}, \quad a_W = 5,\ m_W = 2, \tag{4}$$

where x_b is the released fraction of Q, x_{ig} the ignition angle, $\Delta\varphi_b$ the combustion duration and a_W, m_W the Wiebe parameters [3]. Leakage is described physically: each vane has a sealing perimeter $P_v = 6R_1$ and a clearance δ_s, and the orifice and viscous (Poiseuille) resistances of the gap act in series:

$$\dot{m} = \frac{\dot{m}_o \dot{m}_v}{\dot{m}_o + \dot{m}_v}, \quad \dot{m}_o = \frac{C_d\,\delta_s P_v\,p_u \Psi(p_d/p_u)}{\sqrt{R_g T_u}}, \quad \dot{m}_v = \frac{\delta_s^3 P_v\,(p_u^2 - p_d^2)}{24\,\mu(T_u)\,l\,R_g\,T_u},$$

$$\Psi(r) = \begin{cases} \sqrt{\kappa}\left(\frac{2}{\kappa+1}\right)^{\frac{\kappa+1}{2(\kappa-1)}}, & r \le r_c, \\ \sqrt{\frac{2\kappa}{\kappa-1}\left(r^{2/\kappa} - r^{(\kappa+1)/\kappa}\right)}, & r > r_c, \end{cases} \quad r_c = \left(\frac{2}{\kappa+1}\right)^{\frac{\kappa}{\kappa-1}}, \quad \mu(T) = \mu_0\left(\frac{T}{T_0}\right)^{3/2}\frac{T_0 + S_\mu}{T + S_\mu}, \tag{5}$$

where p_u, T_u and p_d are the upstream and downstream states, C_d = 0.7, l = 2 mm is the seal land length, R_g = 287 J/(kg·K), Ψ is the isentropic flow function of the pressure ratio $r = p_d/p_u$, constant below the critical ratio r_c (choked flow), and μ(T) the viscosity of air by Sutherland's law

with μ_0 = 1.716·10⁻⁵ Pa·s, T_0 = 273.15 K and S_μ = 110.4 K. The expansion chamber leaks into the compression chamber and the exhaust port, the compression chamber into the intake port. The instantaneous gas torque acting on the relative motion of the vanes is

$$M_g = (p_x - p_c)\,\frac{dV}{d\alpha}. \tag{6}$$

For δ_s = 7 μm the mean torque is within 2.5 % of the lumped model with λ = 20 %, but, unlike λ, the leakage now depends on pressure, temperature, stroke duration and engine size. The gap is an effective clearance that represents the leakage past contact (spring-loaded) vane seals, not a machined running clearance; it is a calibration parameter to be identified on a non-firing bench, for example from the pressure decay in a closed chamber. At every dead centre the compression chamber, keeping its state, becomes the expansion chamber and receives Q, and the new compression chamber is filled with fresh charge. As options, the model also contains an ignition delay and the wall heat flux $\dot{Q}_w = h_w A_w (T - T_w)$ with a Woschni-type coefficient h_w scaled by the multiplier C_w [3].

Mechanical model of two shafts

Each shaft has its own angle θ_i, speed ω_i and drive torque τ_i (i = 1, 2). The gas acts on the two vanes of a chamber with equal and opposite torques, and the sign $s = \pm 1$ changes after every stroke because the shafts exchange their roles:

$$\begin{aligned} &J\frac{d\omega_1}{dt} = sM_g + \tau_1, \quad J\frac{d\omega_2}{dt} = -sM_g + \tau_2,\\ &\frac{d\theta_i}{dt} = \omega_i, \end{aligned} \tag{7}$$

With the bisector angle $\theta_b = (\theta_1 + \theta_2)/2$ (the position of the vane pair relative to the housing) and the relative angle $x = s(\theta_1 - \theta_2) + \text{const}$,

$$\begin{aligned} &J\ddot{\theta}_b = \tfrac{\tau_1+\tau_2}{2}, \qquad J\ddot{x} = 2\,(M_g - \bar{M}),\\ &\bar{M} = \tfrac{s(\tau_2-\tau_1)}{2}, \end{aligned} \tag{8}$$

Equation (8) shows that the gas torque acts only on x, whereas the bisector is accelerated only by the common part of the drive torques; if both drives apply equal and opposite torques, the mean speed is invariant. The drive torque that brakes the relative motion must reverse with s every stroke, so each machine works alternately as a generator and as a motor. In the load test an external load torque τ_L on both shafts is added to (7).

Field-oriented control drive model

The most important change compared with [5] is the replacement of the ideal torque source with a physically constrained drive. The causal chain is: torque command → current reference → PI controller → command voltage → limited inverter voltage → current dynamics in the windings → actual current → actual torque → shaft motion. Each shaft carries a surface-mounted PMSM with n_p pole pairs, phase resistance R, inductance L and torque constant K_t. PI current controllers are used because they are the standard current-control structure of FOC drives, including the ODrive controllers [17]. The current references and the PI controllers with decoupling and back-EMF compensation are

$$\begin{aligned} &i_q^* = \text{sat}\left(\tfrac{\tau^*}{K_t}, I_{\max}\right), \quad i_d^* = 0,\\ &v_q^* = K_p \Delta i_q + K_i \xi_q + n_p \omega (L i_d + \psi_m),\\ &v_d^* = K_p \Delta i_d + K_i \xi_d - n_p \omega L i_q, \end{aligned} \tag{9}$$

where $\Delta i = i^* - i$ are the current errors, ξ the integrator states and $\psi_m = K_t/(1.5 n_p)$ the magnet flux linkage, so the effective back-EMF coefficient is $(2/3)K_t$. The gains are defined by the current-loop bandwidth, $K_p = L b_w$ and $K_i = R b_w$, so that the controller zero cancels the electrical pole and the closed loop is a first-order lag [15, 16]. The inverter voltage is limited by the circle of space-vector modulation with d-axis priority, and the integration is stopped while the output is saturated (anti-windup):

$$\begin{aligned} &v_d = \text{sat}(v_d^*, V_{\max}),\\ &v_q = \text{sat}\left(v_q^*, \sqrt{V_{\max}^2 - v_d^2}\right), \quad V_{\max} = \tfrac{V_{bus}}{\sqrt{3}},\\ &\dot{\xi} = \begin{cases} \Delta i, & \text{unsaturated},\\ 0, & \text{saturated}, \end{cases} \end{aligned} \tag{10}$$

Since the windings have inductance, the current cannot change instantaneously. The model is written in the rotor (d–q) frame with an average-value inverter, so the Clarke and Park transformations and the PWM are not modelled explicitly; with amplitude-invariant scaling [14, 16]

$$\begin{aligned} &L\frac{di_d}{dt} = v_d - R i_d + n_p \omega L i_q,\\ &L\frac{di_q}{dt} = v_q - R i_q - n_p \omega (L i_d + \psi_m),\\ &\tau = 3/2\, n_p \psi_m i_q = K_t i_q, \end{aligned} \tag{11}$$

where v_d, v_q and i_d, i_q are the voltages and currents of the d and q axes and τ is the actual motor torque. If the current has not had time to rise or is limited, the motor cannot generate the required torque. The current is reversed physically by the current loop, not by the sign of the mechanical equation as in [6]. Without saturation the closed loop has the step response

$$i_q(t) = i_q^*(1 - e^{-b_w t}), \tag{12}$$

In the baseline simulation the bandwidth is 1000 rad/s (about 159 Hz), so the current loop cannot instantaneously track sharp changes of the gas torque. The controller is continuous or digital with sampling frequency f_s and one-sample delay; a reduced q-axis model and an ideal torque source are kept as options.

Adaptive synchronization algorithm

The synchronization algorithm operates at the outer level: it does not control the current directly, but determines the torque commands passed to the drives. The main quantity is the bisector offset δ_j, the deviation of the mean angular position of the shafts from the ideal periodic position, reduced to ±45°. After each stroke j the algorithm [5] (called algorithm O below) uses the change of kinetic energy $\Delta E_{k,j}$ and the offset to update the torque, applied with equal magnitude to both shafts:

$$\begin{aligned} M_{j+1} &= \frac{A_{ff} - K_{corr}\,\delta_j\,\Delta E_{k,j}}{u_2 - u_1}, \\ \tau^*_{1,2} &= \mp s\,M_{j+1}, \end{aligned} \tag{13}$$

where A_{ff} is the feed-forward cycle work and K_{corr} = 0.3 the correction coefficient. In a steady regime $M_{j+1}(u_2 - u_1)$ equals the gas work W^*, hence

$$K_{corr}\,\delta^* = \frac{A_{ff} - W^*}{\Delta E^*_k}. \tag{14}$$

The residual offset is therefore the value at which the bilinear correction compensates the feed-forward error, inversely proportional to K_{corr}. Because the commands of algorithm O are equal and opposite, the mean speed is not controlled, see (8). In the physical model this proved decisive (Results), and the algorithm was refined by separating the two coordinates of (8) (algorithm P). The stroke ends at the dead centre, the zero crossing of $\dot{x}$, as in free-piston engines [23]; the relative channel makes the drives a virtual viscous coupling, and the bisector channel adds a common torque:

$$\tau^*_{1,2} = \mp c_j\,\frac{\omega_1 - \omega_2}{2} + \frac{s\,D_j}{2}. \tag{15}$$

The coupling coefficient is adapted after every stroke so that the vanes reach the nominal compression:

$$e_j = \frac{x_{\max,j} - u_2}{u_2 - u_1}, \quad c_{j+1} = c_j + |c_j|\left(e^{K_x e_j} - 1\right). \tag{16}$$

so the drive torque passes through zero at each dead centre instead of jumping between $\pm M$. The bisector channel locks θ_b to the stroke clock with the speed error per stroke η_j and the phase set-point δ_{ref} (the vane position relative to the housing, zero in the baseline):

$$\begin{aligned} \eta_j &= \left(\omega_{b,j} - \frac{\pi}{2T_j}\right)T_j, \\ \beta_j &= -\frac{g_1\left(\delta_j - \delta_{ref}\right) + g_2\eta_j + g_3\sigma_j}{T_j^2}, \\ \sigma_{j+1} &= \sigma_j + \delta_j - \delta_{ref}, \quad \sigma_0 = 0, \\ D_{j+1} &= 2J\,s_{j+1}\,\beta_j. \end{aligned} \tag{17}$$

where the angles are in radians and σ_j is the state of the optional integral term (g_3 = 0 except in the load tests). With g_3 = 0, because θ_b is a double integrator of the common torque, the bisector channel is the linear map

$$\begin{bmatrix}\delta \\ \eta\end{bmatrix}_{j+1} = \begin{bmatrix} 1 - g_1/2 & 1 - g_2/2 \\ -g_1 & 1 - g_2 \end{bmatrix}\begin{bmatrix}\delta \\ \eta\end{bmatrix}_j. \tag{18}$$

whose Jury conditions give the stability region; the baseline gains place both poles at 0.5 (g_1 = 0.25, g_2 = 0.875):

$$\begin{aligned} &g_1 > 0, \quad \tfrac{g_1}{2} < g_2 < 2; \\ &g_1 = \left(1 - z_p\right)^2, \quad g_2 = 1 + \tfrac{\left(1 - z_p\right)^2}{2} - z_p^2. \end{aligned} \tag{19}$$

Region (19) is exact for an ideal drive and local for the real one. A constant load torque leaves the offset $-\tau_L T^2/(J g_1)$, which the integral term of (17) with $g_3 > 0$ removes. For the relative channel, identification of the simulator by step responses gives a second-order model $e_{j+1} = a_1 e_j + a_2 e_{j-1} + b_0 y_{j+1} + b_1 y_j$ with $y_j = \ln(c_j/c^*)$; together with the linearized adaptation (16), $y_{j+1} = y_j + K_x e_j$, the closed loop is of third order, and under the assumptions $b_0 + b_1 < 0$, $b_1 - b_0 > 0$, $|a_2| < 1$ its Jury conditions are

$$\begin{aligned} &0 < K_x < \tfrac{2(1 + a_1 - a_2)}{b_1 - b_0}, \\ &|a_1(1 + a_2) - K_x(b_1 - a_2 b_0)| < 1 - a_2^2. \end{aligned} \tag{20}$$

Formal synchronization criterion

A run of 60 strokes is classified by the last 10 strokes: **S** (stable synchronization) if all strokes are completed without vane contact, $|\delta_j - \delta_{ref}| \le 5°$, the offset changes by at most 0.05° per stroke, the stroke duration by at most 0.5 % and less than 0.1 % of the steps are saturated; **M** if only the saturation condition fails; **T** if the phase is within 5° but not settled; **L** (loss of synchronization) otherwise; a run for which the calibration finds no periodic stroke (the drive cannot balance the gas work) is also assigned class L. The admissible working volume is the largest V_s of class S on a uniform grid with a step of 0.5 cm³. The drive is characterized by the torque reserve and the peak-to-mean ratio, the loop-time ratio and the voltage reserve:

$$\Lambda = \frac{K_t I_{\max}}{\bar{M}}, \quad \chi = \frac{K_t I_{pk}}{\bar{M}}, \qquad \Pi = \frac{1}{b_w T}, \quad \Upsilon = \frac{V_{\max}}{V_{pk}}, \tag{21}$$

where $\bar{M}$ is the mean drive torque, T the stroke duration and I_{pk}, V_{pk} the peak magnitudes of the current and voltage vectors. The margins $I_{\max}/I_{pk} = \Lambda/\chi > 1$ and $\Upsilon > 1$ are necessary but not sufficient conditions of synchronization.

Numerical method and software implementation

The system is hybrid: continuous dynamics within a stroke and events at the dead centres. It is integrated with a fixed step Δt = 0.5 μs, three orders of magnitude below L/R: the speeds, currents and chamber states by the explicit Euler method and the angles by the trapezoidal rule; events are located by linear interpolation. In each run the program computes the geometry (1), (2), finds the initial periodic orbit by calibration of one stroke, presets the PI integrators to their steady values, integrates (3)–(11) and, at each dead centre, measures the stroke quantities, updates the algorithm by (13) or (15)–(17), swaps the chambers and releases the heat; the run is then classified by the formal criterion. The simulator is a single HTML file in JavaScript; the same model core is used by the browser interface and by a Node.js batch runner, and a 60-stroke run takes about 1.7 s. About 700 runs were performed; the code and the experiment files with all parameters and initial conditions are available on request (see Data availability).

Description of the simulator software interface

Fig. 2 shows the interface of the simulator. The input panels (Fig. 2a) specify the drive (motor preset, K_t, pole pairs, R, L, $I_{\max}$, V_{bus}, bandwidth, drive model and sampling frequency), the engine and working fluid (volume, compression ratio, temperature rise, heat release, leakage model, seal gap and flywheel) and the synchronization algorithm (law, gains, time step, number of strokes and scenario; the load-step amplitude τ_L is used only in the load-step scenario). The results panel (Fig. 2b) shows the regime class, the indicators (21), the speed, power, peak current and voltage, plots of the per-stroke quantities and of the torques, pressures and currents within a stroke, and exports the per-stroke table. The simulator thus allows the influence of the geometry, gas cycle and drive parameters on synchronization to be evaluated before a laboratory test bench is built.

RESEARCH RESULTS

Based on the described mathematical model, a computer program was developed that calculates the behaviour of the system step by step. The calculations showed that, for the selected industrial motor M8325s, the working-chamber volume that the system synchronizes stably in the butane combustion mode lies between 2.5 and 5 cm³, including the baseline 4.0 cm³. A further increase of the scale leads to loss of synchronization because of the current limit, and a decrease because of leakage. Tables 1 and 2 present the system parameters used in the experiments; the motor constants are taken from the manufacturer's data, and leakage is defined by the seal gap.

Verification of the model

Since no measurements on an electromagnetically synchronized engine exist yet, the model was verified rather than validated (Table 3). V1 checks only the implementation and V5 only the constants; the other tests use independent references: analytical solutions, the ideal Otto cycle, energy balances and re-implemented blocks. All criteria are met, but this does not replace a physical validation.

For algorithm P the stroke duration, current and torque converge with the step, while the residual offset varies non-monotonically within 0.002–0.048°, so it is resolved only as |δ| < 0.05°. For algorithm O Richardson extrapolation gives a step-independent offset of 1.16° (1.25° at Δt = 0.5 μs). With the legacy options (lumped λ = 20 %, torque sign flipped in the mechanics) the results of [6] are reproduced to four digits and the phase within 0.04°.

Baseline regime and dynamics of synchronization parameters

Table 4 presents a fragment of the numerical data of the synchronization process in the baseline regime. The data confirm the gradual stabilization of the parameters and the absence of current or voltage saturation. While the coupling coefficient adapts from its initial value, the stroke duration changes from 7.45 to 7.19 ms and the offset reaches −4.1°; then both converge, and from stroke 32 the offset stays below 0.05°.

Table 1. **Drive parameters (ODrive data [17])**

Parameter	Symbol	M8325s 100KV (baseline)	D6374 150KV	D5065 270KV	Unit
Torque constant	K_t	0.0827	0.055	0.031	N·m/A
Phase resistance	R	0.024	0.039	0.039	Ω
Phase inductance	L	9.9	24	16	μH
Pole pairs	n_p	20	7	7	–
Current limit (forced air, amplitude)	$I_{\max}$	60	70	65	A
Maximum torque	$K_t I_{\max}$	4.96	3.85	2.02	N·m
DC bus voltage / voltage limit	V_{bus} / $V_{\max}$	56 / 32.3	56 / 32.3	56 / 32.3	V
Current-loop bandwidth	b_w	1000	1000	1000	rad/s
PI gains	K_p / K_i	0.0099 / 24	0.024 / 39	0.016 / 39	V/A, V/(A·s)
Controller	–	continuous; digital f_s = 8–40 kHz studied			–

***Source*: compiled by the authors**

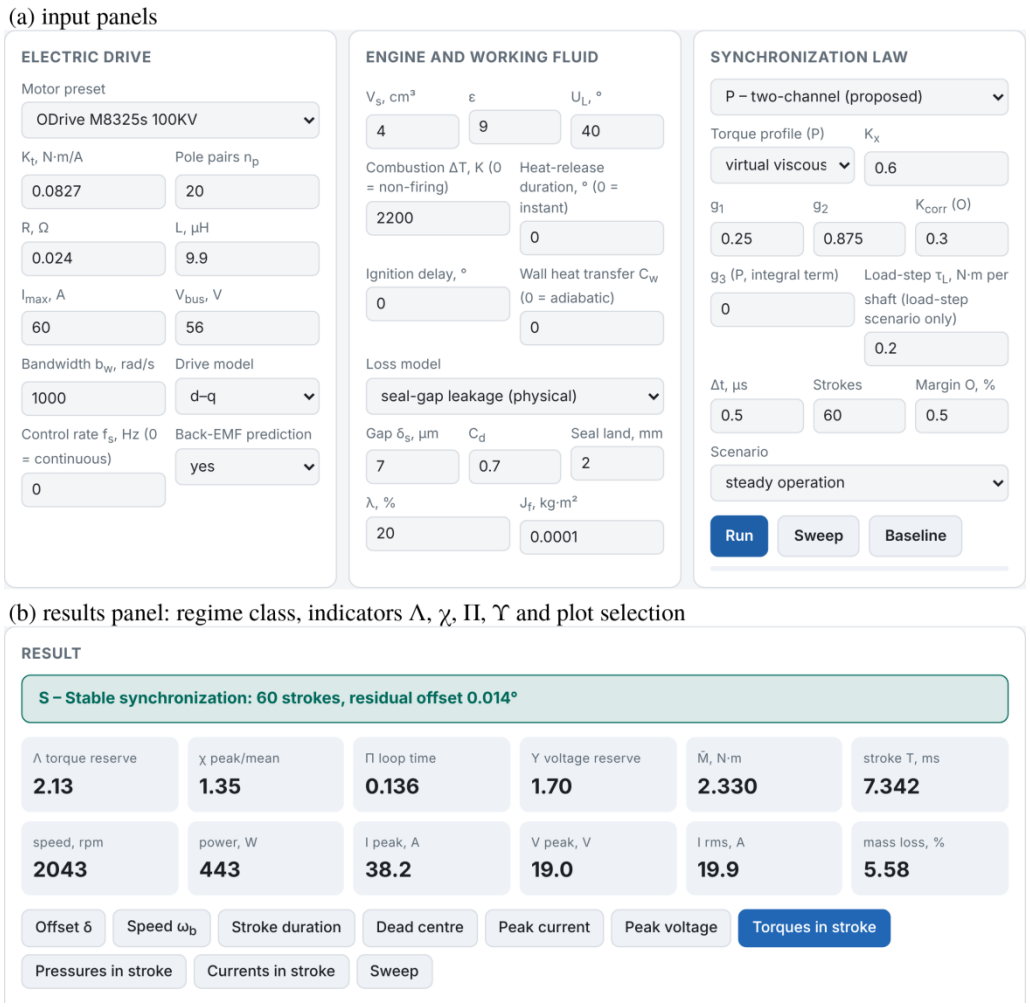


Fig. 2. **Interface of the simulator: (a) input panels; (b) results panel of the baseline regime with the regime class, indicators (21) and plot selection**

***Source*: compiled by the authors**

Table 2. **Engine, working-fluid and algorithm parameters (baseline)**

Parameter	Value	Parameter	Value
Working-sector volume V_s	4.0 cm³	Exponent κ, gas constant R_g	1.3; 287 J/(kg·K)
Vane size U_L, compression ratio ε	40°; 9	Intake p_{at}, T_{at}	100 kPa; 300 K
R_1 / R_2 / h	6.59 / 19.78 / 13.18 mm	Temperature rise ΔT (firing / non-firing)	2200 K / 0 K
$dV/d\alpha$; seal perimeter P_v	2.29 cm³/rad; 39.6 mm	Heat release	instantaneous (Wiebe studied)
Flywheel J_f; total J	$1.0\cdot10^{-4}$; $1.217\cdot10^{-4}$ kg·m²	Seal gap δ_s; C_d; land l	7 μm; 0.7; 2 mm
Algorithm P: K_x; g_1; g_2	0.6; 0.25; 0.875	Algorithm O: K_{corr}; feed-forward margin	0.3 deg^{-1}; 0.5 %
Time step Δt; strokes N	0.5 μs; 60	Criterion window N_w; wall heat transfer C_w	10 strokes; 0 (adiabatic)

***Source*: compiled by the authors**

Table 3. **Verification tests with acceptance criteria**

Test	Reference	Criterion	Result
V1. Closed chamber without leakage and heat release	Polytrope pV^{κ} = const	≤ 10^{-9}	$6.7\cdot10^{-16}$
V2. Current step 0→20 A	Response (12)	≤ 0.1 %	0.027 %
V3. Mechanical energy over 60 strokes	Gas work = drive work + Δ kinetic energy	≤ 0.1 %	0.034 %
V4. Electrical energy of each drive	Copper loss + mechanical + Δ magnetic	≤ 0.01 %	< 10^{-6} %
V5. No-load speed from $V_{\max}$, $K_e = (2/3)K_t$	Rating KV·V_{bus} = 5600 rpm	≤ 1 %	5600 rpm
V6. Time step 4 → 0.125 μs, algorithm P	Δt = 0.125 μs	T, I_{pk}, $\bar{M}$ ≤ 1 %	≤ 0.26 %; δ: 0.002–0.048°
V7. Legacy options of [6]	Published 8.49 ms, 27.50 A, −1.21°	≤ 0.1 %; δ within spread	four digits; −1.25°
V8. Zero initial PI integrators	Preset integrators	no anomalous stroke	809.7 ms → 8.2 ms
V9. Reduced q-axis model	Full d–q model	T, I_{pk} ≤ 0.5 %	equal T and I_{pk}
V10. Blowdown through the seal gap	Choked-flow solution; LSODA in p, m	≤ 0.1 %	0.013 %; 0.0008 %
V11. Drive, reversing command, V_{bus} = 56/20 V	Independent RK4 code	≤ 0.5 %	0.013 %; 0.13 % (saturated)
V12. Cycle without leakage, instantaneous heat release	Ideal Otto cycle [3]	≤ 0.1 %	work $3\cdot10^{-6}$ %, $p_{\max}$ $3\cdot10^{-5}$ %

***Source*: compiled by the authors**

Table 4. **Dynamics of synchronization parameters by stroke (baseline regime, δ_s = 7 µm, algorithm P)**

Stroke	Duration, ms	Offset δ, °	I_{pk}, A	V_{pk}, V	ω_b, rad/s
1	7.451	0.016	36.35	18.69	210.86
2	7.270	−2.153	36.96	18.90	210.82
3	7.228	−3.928	38.71	19.08	215.85
4	7.194	−4.094	38.46	19.37	219.80
5	7.201	−3.031	38.23	19.57	221.35
…	…	…	…	…	…
56	7.342	0.017	38.17	19.00	213.93
57	7.342	0.017	38.17	19.00	213.93
58	7.342	0.015	38.17	19.00	213.93
59	7.342	0.014	38.17	19.00	213.93
60	7.342	0.014	38.17	19.00	213.93

Source: compiled by the authors

The steady stroke lasts 7.342 ms (2043 rpm), and the dead centre is held at 90.000°. Zero initial values of the PI integrators produce a non-physical transient: the current falls from 29 to 16 A within 0.8 ms, the vanes almost stop and the second stroke lasts 809.7 ms (test V8); therefore the integrators are preset to their steady values. With the integrators preset to their steady values, all strokes of that model last about 8.2 ms; this initialization is used in all runs. In the baseline regime the peak pressure is 85.8 bar and the gas torque varies within the stroke from +19.4 to −4.4 N·m, while the drive torque follows a smooth viscous profile with a mean of 2.330 N·m (Fig. 3a). The peak current is 38.2 A (64 % of $I_{\max}$) and the peak voltage 19.0 V, so Λ = 2.13, χ = 1.35, Π = 0.136 and Υ = 1.70. The q-axis current changes sign every stroke (Fig. 3b). With a constant torque per stroke, as in the earlier model [6], the actual torque has the wrong sign while the gas impulse is maximal, which raises the mean torque to 3.205 N·m.

Behaviour of the original algorithm and influence of the drive constraints

To check whether the residual offset of algorithm O is caused by the physical limitations of the drive, algorithm O was run with the lumped leakage and a calibrated feed-forward with a 0.5 % margin (Fig. 4), because in the physical model it does not settle (Table 5). Over K_{corr} = 0.1–0.9 the product $K_{corr}\delta^*$ stays equal to 0.479 (Fig. 4a), as predicted by (14), and the offset is the same for the ideal and the constrained drive (1.598° and 1.597°). It is therefore a steady-state error of the correction law rather than a consequence of the drive physics. After a speed disturbance the mean speed under algorithm O does not return (Fig. 4b, c), whereas algorithm P recovers.

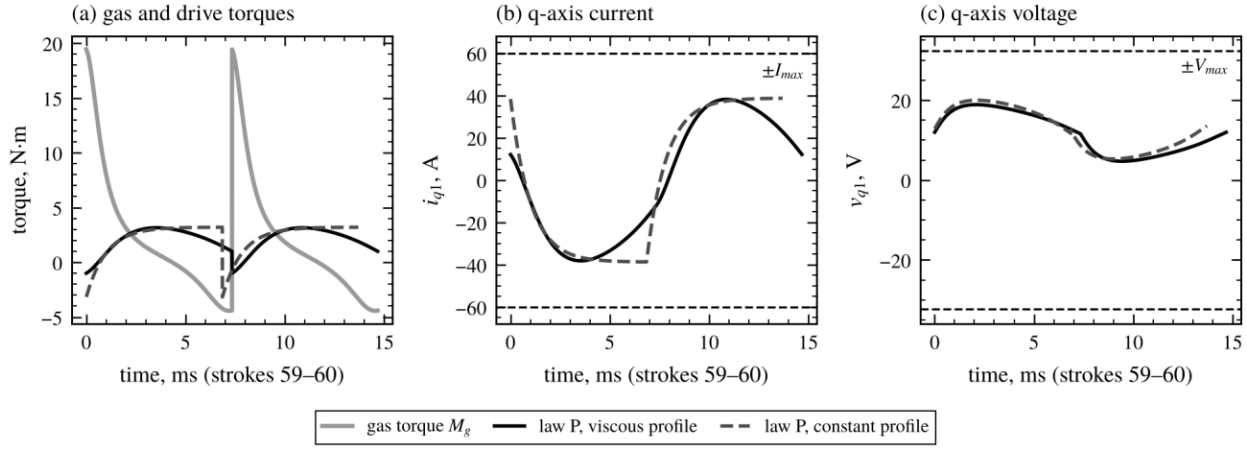


Fig. 3. **Baseline regime, strokes 59–60: (a) gas torque and drive torque for the viscous and constant profiles; (b) q-axis current and (c) q-axis voltage of drive 1**

***Source*: compiled by the authors**

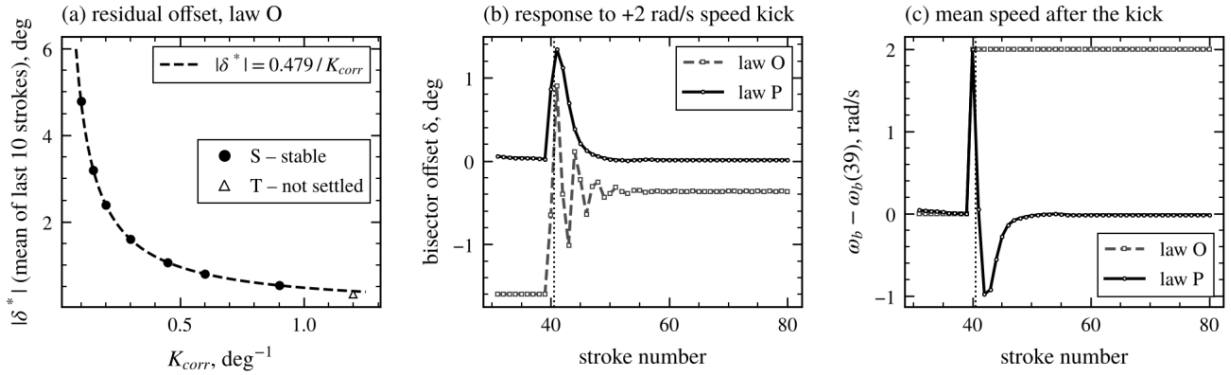


Fig. 4. **Original algorithm O: (a) residual offset versus correction coefficient with the dependence (14); (b) bisector offset and (c) mean speed after a speed disturbance of +2 rad/s at stroke 40 for algorithms O and P**

***Source*: compiled by the authors**

Table 5 removes the idealizations of the earlier model [6] one by one (level L0 uses its closed-form feed-forward instead of the calibrated one, hence its offset of 1.25° instead of 1.60°): algorithm O loses synchronization when the torque reversal is formed by the current loop (L1) and immediately with the physical leakage (L2), whereas algorithm P stays stable at every level; at level L0 it reduces the residual offset from 1.25° to 0.012°. With signed currents algorithm O requires $b_w \geq 2000$ rad/s ($\Pi \leq 0.07$) and algorithm P works from 700 rad/s ($\Pi \leq 0.2$). With a digital controller algorithm P is stable for f_s = 8–40 kHz, with residual offsets of 0.40° at 8 kHz, 0.09° at 16 kHz and below 0.05° from 24 kHz.

Influence of gas leakage

To analyse stability, the influence of gas leakage was investigated with the seal gap δ_s varied from 0 to 12 μm, which covers the lumped coefficient λ = 0–40 % of the earlier model [6] (Fig. 5a). The mean drive torque decreases from 3.043 N·m without leakage to 2.330 N·m at 7 μm and 1.267 N·m at 10 μm, and the mass lost per expansion grows to 7.6 % (Fig. 5b). Unlike the lumped coefficient, the physical leakage changes the stability (Fig. 5c): algorithm P is stable for δ_s = 0–9 μm; algorithm O, even with an ideal drive, only for $\delta_s \leq 2$ μm, and the constant profile of algorithm P only for 7–9 μm, because it needs the dissipation provided by the leakage.

A finite heat release over 10–40°, an ignition delay of 5–15° and wall heat transfer (C_w = 0.5–2, 10–31 % of the heat) reduce the mean drive torque by up to 39, 29 and 23 %, respectively; all these regimes remain stable, and the absolute torques and currents are model predictions.

Admissible working-chamber scale and the non-firing mode

Fig. 6a shows the peak current versus the working volume for three ODrive motors on a uniform grid of 1–8 cm³. From above the range is limited by the current: at its upper end $I_{\max}/I_{pk}$ = 1.17 for M8325s (51.5 A at 5 cm³) and 1.22 for D6374 (57.4 A at 4 cm³); beyond it synchronization is lost (M8325s) or settles only with saturation of the current reference, class M (D6374 at 4.5 cm³, D5065 at 3 cm³).

Table 5. **Removing the idealizations of the earlier model [6] one by one**

Model level	Algorithm O: class, δ*, I_{pk}	Algorithm P: class, δ, I_{pk}
L0. Earlier model [6]: lumped λ = 20 %, q-axis model, torque sign flipped in mechanics	S, −1.25°, 27.5 A	S, 0.012°, 34.8 A
L1. + physically signed currents (torque reversal through the current loop)	L at stroke 8	S, 0.014°, 37.0 A
L2. + seal-gap leakage, δ_s = 7 μm	L at stroke 2	S, 0.014°, 38.2 A
L3. + full d–q model	L at stroke 2	S, 0.014°, 38.2 A
L4. + digital control, f_s = 16 kHz, delay, back-EMF prediction	L at stroke 2	S, 0.08°, 38.8 A

***Source*: compiled by the authors**

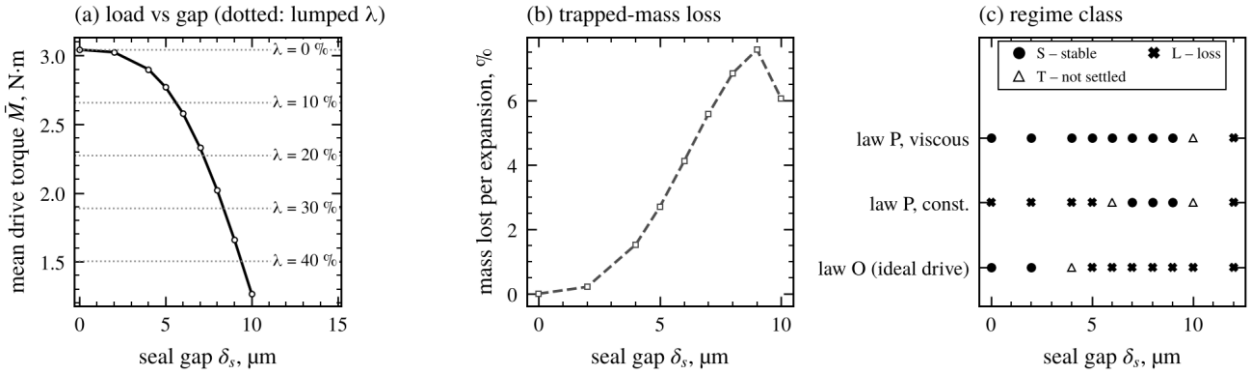


Fig. 5. **Influence of the seal gap: (a) mean drive torque compared with the lumped coefficient λ (dotted); (b) mass lost per expansion; (c) regime class for algorithm P with the viscous and constant profiles and for algorithm O (S – stable, T – not settled, L – loss of synchronization)**

***Source*: compiled by the authors**

From below the range is limited by leakage, because the seal perimeter scales only as $V_s^{1/3}$. The upper end is about 1.7 times lower than the estimate of 8.7 cm³ in [6] (dotted line), which neglected the torque reversal and the scale dependence of leakage. The whole range refers to the baseline effective gap of 7 μm: for 10 and 12 μm the stable range shifts to 5–6.5 and 6.5–7.5 cm³, and for 15 μm no volume up to 8 cm³ is stable.

To additionally verify the operability of the model, a non-firing mode (ΔT = 0) with the baseline parameters was studied: the drives keep the vanes synchronous while the trapped air is compressed and expanded, as on a bench without a combustion system. Without combustion algorithm P remains stable up to the largest studied volume of 300 cm³ with a peak current of only 23.2 A (Fig. 6b), whereas the legacy algorithm O loses synchronization above 100 cm³. This confirms that the admissible engine scale depends significantly on the nature of the gas load, not only on the maximum torque of the drive.

Stability of the refined algorithm

Region (19) was confirmed on 110 gain pairs with an ideal drive: all 58 pairs inside it gave stable synchronization, all 47 outside it did not, and the 5 pairs on the boundary $g_2 = g_1/2$, where a pair of poles lies on the unit circle, gave classes S or T; with the real drive the effective gains are reduced by about $1 - \Pi$, so (19) is a local condition. For the relative channel, step responses identified a second-order model ($a_1 = -0.213$, $a_2 = 0.437$, $b_0 = -0.225$, $b_1 = 0.060$, $R^2 = 0.99993$), for which the first condition of (20) gives $K_x < 2.46$ and the second one $K_x < 3.18$, so the first is binding; in runs of 300 strokes a flip bifurcation occurs between $K_x = 2.3$ and 2.4, about four times above the baseline $K_x = 0.6$. Both channels are needed: without the bisector channel the phase drifts by more than 5° within four strokes, and with a fixed coupling coefficient ($K_x = 0$), i.e. a cross-coupling damping with a constant gain, the dead centre settles at 90.74° and drifts to 87.1° after a 20 % drop of ΔT (+29 % of the chamber volume at the dead centre), whereas with the adaptation (16) it returns to 89.96°.

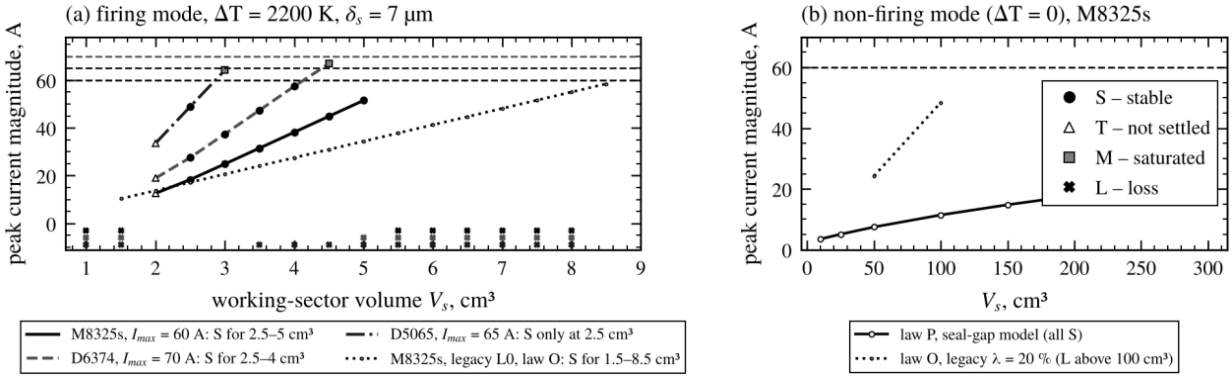


Fig. 6. **Peak current versus working-sector volume: (a) firing mode for three motors (dashed lines – current limits) and the legacy model of [6]; (b) non-firing mode for the M8325s motor; markers – regime class**

***Source*: compiled by the authors**

Dynamic regimes, load changes and operating range

A 20 % drop of ΔT at stroke 30 lengthens the stroke from 7.34 to 7.93 ms, and the phase channel returns the offset to zero after a transient of up to 19.5° (Fig. 7a, b). A complete misfire produces one stroke of 13.4 ms and a transient of 27.3°, after which the offset is below 0.5° within 37 strokes; a 3° step of δ_{ref} is tracked without current overshoot. Algorithm O (with the settings of Fig. 4) loses synchronization in the first disturbed stroke, even for a 2.3 % drop of ΔT. In a Monte-Carlo test with random initial conditions and drive parameters algorithm P was stable in 50 of 50 cases, algorithm O with an ideal drive in 16 of 50. With the proportional bisector channel a step of the external load τ_L (Fig. 7c) leaves the offset $-\tau_L T^2/(Jg_1)$ (−5.06° and −20.3° for 0.05 and 0.2 N·m); with the integral term of (17) (g_1 = 0.6875, g_2 = 1.15625, g_3 = 0.125; all three poles at 0.5) the offset returns below 0.5° within 7–12 strokes for 0.05–0.4 N·m.

Stable synchronization was also observed from motoring through idle (ΔT ≈ 175 K, about 1220 rpm) to full load, with a smaller flywheel up to about 3150–3190 rpm, where the voltage reserve is exhausted, and during ramps of ΔT by 50 %. A ±20 % variation of the drive, inertia, heat-release and seal parameters did not change the class of the baseline regime.

DISCUSSION OF RESULTS

The current implementation solves the main problem of this work: it replaces ideal torque application with a physically realistic FOC drive model that includes limitations on current, voltage, inductance, resistance, back-EMF and current-loop bandwidth, and it describes the leakage through the seals physically. The model has been verified (Table 3), but not yet validated against measurements; its range of applicability is summarized in Table 6.

The obtained results refine the initial idea of the paper: electric machines can indeed act as shaft synchronizers, but the limit of their applicability is determined not only by the maximum torque.

The rate at which this torque is generated, i.e. the current-loop bandwidth relative to the stroke frequency, is also important: when the torque reversal is formed by the current loop, the loop must be at least five times faster than the stroke for algorithm P and fourteen times for algorithm O.

Therefore, a correct model must include R, L, K_t, back-EMF, voltage limitation and anti-windup, and the sign of the drive torque must be determined by the current.

The non-firing mode is the most appropriate for the first test bench. It preserves the main synchronization problem, the reversal of the drive torque at every stroke and the coupling of the vanes only through the gas, but removes the combustion impulse: the predicted peak current stays below 23.2 A up to 300 cm³. This makes it possible to move from impractical centimetre-scale dimensions to a laboratory engine with a housing diameter of about 86 mm ($V_s \approx 41$ cm³) and to validate the drive and leakage blocks before firing tests.

Leakage should not be regarded as a stabilizing factor in general: it reduces the mean drive load (Fig. 5a) and provides the dissipation needed by a constant torque profile, but the original algorithm cannot tolerate the physical leakage, and the viscous profile provides its own dissipation. In a power-producing machine leakage reduces efficiency, and it also limits the admissible scale from below.

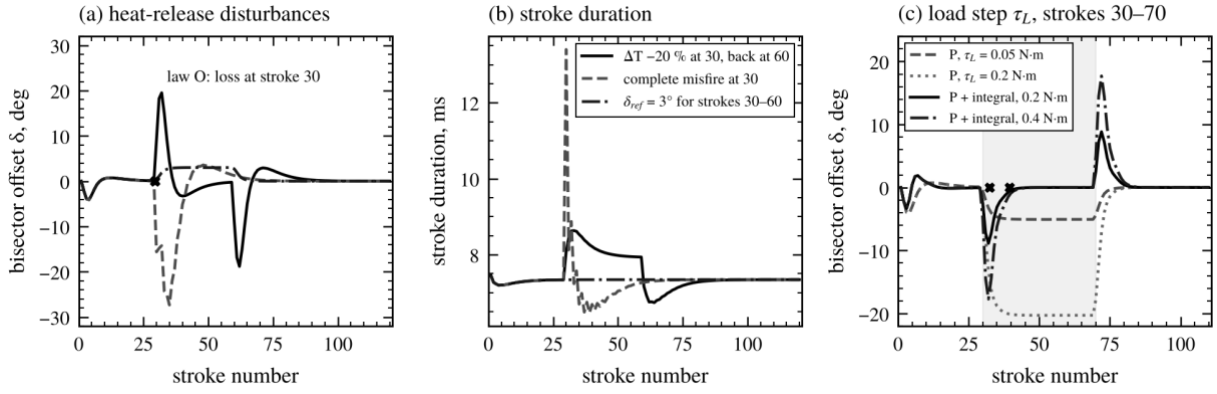


Fig. 7. **Dynamic regimes of algorithm P: (a) bisector offset and (b) stroke duration for a −20 % step of ΔT at stroke 30 restored at stroke 60, a complete misfire and a 3° set-point step; (c) bisector offset for load-torque steps with the proportional channel and with the integral term (g_1 = 0.6875, g_2 = 1.15625, g_3 = 0.125); crosses – loss of synchronization by algorithm O**

Source: compiled by the authors

Table 6. **Range of applicability of the model and of the results**

Factor	Representation in the model	Studied range; consequence
Speed and voltage	back-EMF, voltage circle $V_{bus}/\sqrt{3}$, no field weakening	1110–3450 rpm; stable up to about 3190 rpm (M8325s, 56 V)
Current, torque, magnets, heating	current limit, constant K_t, R; no saturation, demagnetization or thermal model	valid while $I_{pk} < I_{\max}$; −20 % of K_t: 47.7 A, stable; copper loss ≈ 28.5 W per motor
Inverter, sensors, mechanics	average-value inverter, ideal encoders, rigid shafts without friction	no PWM ripple, dead time or noise; friction asymmetry disturbs the bisector channel
Chambers and combustion	single zone, κ = 1.3, instantaneous or Wiebe release; optional wall heat and ignition delay	$p_{\max} \le 90$ bar, ΔT = 0–2200 K; pressure traces are qualitative
Seals and scale	orifice and viscous flow (5), constant gap; fixed proportions (1), (2)	δ_s = 0–12 μm (effective gap, calibration parameter); V_s = 1–8 cm³ firing, 10–300 cm³ non-firing

***Source*: compiled by the authors**

The residual offset of algorithm O (about 1.6° with the settings of Fig. 4) is not the price paid for the physical realizability of the model but the equilibrium (14) of the bilinear correction law: it is the same for the ideal and the constrained drive, and the 0.006° of [5] refers to a larger engine. The refined algorithm separates the two coordinates of (8): the relative channel regulates the dead centre and the bisector channel the phase of the vanes relative to the housing. This transfers the principle of free-piston engine generators, in which the machine acts as a velocity-proportional damping that controls the dead centre [23–25]; in terms of multi-motor synchronization [20–22], the relative channel is a cross-coupling term and the bisector channel a virtual master defined by the stroke clock, but this comparison is qualitative: a quantitative comparison with tuned cross-coupled or virtual-shaft controllers, like the physical validation, remains a task for further work.

At the same time, predictive control is not implemented in the current version: the current loop is a reactive PI controller that responds to the current error rather than predicting the gas impulse. Therefore, the results should be interpreted as a verification of the operability of FOC-limited synchronization rather than as a final optimal control law. The admissible volumes, thresholds and currents are model predictions under the assumptions of Table 6, intended for screening and the planning of experiments.

CONCLUSIONS

1. This work developed a coupled computer model for synchronizing the shafts of a rotary vane internal combustion engine, combining the mechanical dynamics of two shafts, the variable gas torque in the working chambers with pressure-dependent leakage through the seals, and a physically constrained electric-drive model. The control electric machines are not treated as ideal torque sources, but are described through current dynamics, inductance, winding resistance, back-EMF, current limitation, inverter voltage limitation and finite current-loop bandwidth. The model meets the acceptance criteria of all verification tests; its validation against measurements remains a task for further work.

2. An FOC drive model was implemented in which the desired torque is first converted into the desired q-axis current, after which the actual torque, including its reversal at every stroke, is formed through the current PI controller and the electrical dynamics of the windings. In this model the original stroke-level algorithm loses synchronization, and its residual offset of about 1.5° is a steady-state error of the correction law. The algorithm was therefore refined by separate regulation of the dead centre and of the bisector phase with local stability conditions; the refined algorithm keeps the offset below 0.05° in the baseline regime with a continuous controller (0.09–0.40° with a digital controller at 16–8 kHz) and maintains synchronization after misfires and changes of heat release and load.

3. It was shown that the limiting factor of synchronization is not only the maximum electromagnetic torque of the motor, but also the rate at which this torque is formed, determined by the current-loop bandwidth relative to the stroke frequency, the winding inductance, the available inverter voltage and the back-EMF. The current and

voltage margins are necessary but not sufficient conditions of synchronization.

4. For the baseline mode simulating butane combustion, stable synchronization of a laboratory model with a working volume of one chamber of 4.0 cm³ was demonstrated: the mean drive torque is 2.33 N·m, and the motor with a maximum torque of about 5 N·m uses 64 % of its current limit. For this motor the admissible volume on the studied grid is about 2.5–5 cm³ at the baseline effective seal gap of 7 μm; it is limited by the current from above and by leakage from below.

5. Gas leakage through the vane seals reduces the peak pressure and the mean load on the electric drive, but it is not in general a stabilizing factor: it is needed by a constant torque profile, whereas the original algorithm loses synchronization with the physical leakage model. This effect may be useful at the stage of experimental verification of synchronization, but not in terms of the energy efficiency of the engine.

6. An additional numerical experiment without combustion showed that the admissible scale of the working chamber depends significantly on the nature of the gas load: in this mode the drive is sufficient for all studied volumes up to 300 cm³, which makes the non-firing mode appropriate for a laboratory test bench and for the preliminary verification of the synchronization algorithm.

7. The proposed model can be used as a tool for the preliminary screening of designs of rotary vane engines with electromagnetic shaft synchronization. It makes it possible, before physical experiments, to evaluate the admissible geometry scale, the influence of the electric-drive parameters, the approach to current and voltage limitations and the stability of synchronization under different gas-load modes; its quantitative results are model predictions within the limits of Table 6, and the drive and leakage blocks are to be validated on a non-firing test bench.

Conflicts of interest: The authors declare that they have no conflicts of interest, financial, personal, authorship or other, that could have influenced the research and the results reported in this paper

Funding: The research was carried out without financial support

Data availability: The simulator code, the experiment configurations and the stored results are available from the corresponding author upon reasonable request

Use of artificial intelligence tools: During the preparation of the manuscript**,** the authors used the AI assistant Claude (Anthropic) to help refactor the simulator code and edit the language of the text. All equations, code, numerical results and conclusions were checked by the authors, who take full responsibility for the content of the article

REFERENCES

1. Gao, J., Tian, G., Jenner, P., Burgess, M. & Emhardt, S. “Preliminary explorations of the performance of a novel small scale opposed rotary piston engine”. *Energy*. 2020; 190: 116402. DOI: https://doi.org/10.1016/j.energy.2019.116402.

2. Wang, Y., Gao, J., Zhao, Y., Huang, J., Song, J., Fu, Z. & Yang, C. “Kinematics characteristics of opposed rotary piston engine”. *Transactions of Beijing Institute of Technology*. 2024; 44 (4): 369–376 (in Chinese). DOI: https://doi.org/10.15918/j.tbit1001-0645.2023.113.

3. Heywood, J. B. “Internal combustion engine fundamentals”. *2nd ed. McGraw-Hill Education. New York*. 2018.

4. Galin, A., Galin, O., Galin, N. & Galin, V. “Electromagnetic only vane coordination of a cat and mouse engine”. *Pat. US 10,472,965 B2. IPC F01C 1/063; F01C 20/08; F04C 2/063; F04C 23/02*. 2019. – Available from: https://patents.google.com/patent/US10472965B2. – [Accessed: 24 Oct 2026].

5. Ushenko, Y. O., Uhryn, D. I., Karachevtsev, A. O., Halin, Y. O. & Ilin, V. A. “Method for automated control of rotor engine blade synchronization”. *Applied Aspects of Information Technology*. 2025; 8 (3): 334–347. DOI: https://doi.org/10.15276/aait.08.2025.22.

6. Halin, Y. O., Shevchuk, S. F. & Blyzniuk, M. M. “Computer model of rotary-vane engine shaft synchronization under physical electric-drive constraints”. *Informatics. Culture. Technology*. 2026; 3 (2): 1047–1056. DOI: https://doi.org/10.15276/ict.03.2026.81.

7. Mirzaei, M., Hashemi, S. M., Saranjam, B. & Binesh, A. “Two-zone simulation of an axial vane rotary engine cycle”. *International Journal of Applied Mechanics and Engineering*. 2021; 26 (2): 143–159. DOI: https://doi.org/10.2478/ijame-2021-0024.

8. Kim, Y.-J., Yoon, A.-S. & Lee, C.-E. “Validation of CFD analysis on flow and combustion characteristics for a GP3 rotary engine”. *Energies*. 2025; 18 (4): 758. DOI: https://doi.org/10.3390/en18040758.

9. Dong, W. & Bedekar, V. “Design, modeling, and feasibility analysis of rotary valve for internal combustion engine”. *Journal of Combustion*. 2024; 2024: 8049436. DOI: https://doi.org/10.1155/2024/8049436.

10. Dudás, L. “Developing a rotary internal combustion engine characterized by high speed operation”. In *Vehicle and Automotive Engineering. Lecture Notes in Mechanical Engineering*. *Springer,* Cham. 2017. DOI: https://doi.org/10.1007/978-3-319-51189-4_8.

11. Shen, X. & Costall, A. W. “Enhancing the efficiency of rotary thermal propulsion systems”. *Energies*. 2024; 17 (9): 2112. DOI: https://doi.org/10.3390/en17092112.

12. Yang, Z., Ji, C., Huang, X., Yang, J., Wang, H. & Wang, S. “Modeling and analysis of apex seal leakage in a hydrogen fueled Wankel rotary engine”. *Fuel*. 2023; 331: 125848. DOI: https://doi.org/10.1016/j.fuel.2022.125848.

13. Savvakis, S., Mertzis, D., Nassiopoulos, E. & Samaras, Z. “A design of the compression chamber and optimization of the sealing of a novel rotary internal combustion engine using CFD”. *Energies*. 2020; 13 (9): 2362. DOI: https://doi.org/10.3390/en13092362.

14. Pillay, P. & Krishnan, R. “Modeling, simulation, and analysis of permanent-magnet motor drives. Part I: The permanent-magnet synchronous motor drive”. *IEEE Transactions on Industry Applications*. 1989; 25 (2): 265–273. DOI: https://doi.org/10.1109/28.25541.

15. Boldea, I. & Nasar, S. A. “Electric drives”. *3rd ed. CRC Press. Boca Raton*. 2016. DOI: https://doi.org/10.1201/9781315368573.

16. Sul, S.-K. “Control of electric machine drive systems”. *Wiley-IEEE Press*. *Hoboken*. 2011. DOI: https://doi.org/10.1002/9780470876541.

17. ODrive Robotics. “ODrive motors”. ODrive documentation. – Available from: https://docs.odriverobotics.com/v/latest/hardware/odrive-motors.html. – [Accessed: 24 Jul 2026].

18. Dai, S., Wang, J. B., Sun, Z. & Chong, E. “Deadbeat predictive current control for high-speed permanent magnet synchronous machine drives with low switching-to-fundamental frequency ratios”. *IEEE Transactions on Industrial Electronics.* 2022; 69 (5): 4510–4521. DOI: https://doi.org/10.1109/TIE.2021.3078383.

19. Havrylenko, O. & Kulinich, S. “Analyzing an error in the synchronization of hydraulic motor speed under transient operating conditions”. *Eastern-European Journal of Enterprise Technologies*. 2019; 4 (7 (100)): 30–37. DOI: https://doi.org/10.15587/1729-4061.2019.175033.

20. Wang, S., Chen, Y. & Zhang, G. “Adaptive fuzzy PID cross coupled control for multi-axis motion system based on sliding mode disturbance observation”. *Science Progress*. 2021; 104 (2). DOI: https://doi.org/10.1177/00368504211011847.

21. Zhang, X., Hu, H., Wang, H. & Wang, Z. “Overview of position synchronous control technology for multi-motor system”. *Systems Science & Control Engineering*. 2024; 12 (1): 2427074. DOI: https://doi.org/10.1080/21642583.2024.2427074.

22. Lan, C.-Y., Wang, H., Deng, X., Zhang, X.-F. & Song, H. “Multi-motor position synchronization control method based on non-singular fast terminal sliding mode control”. *PLoS ONE*. 2023; 18 (6): e0281721. DOI: https://doi.org/10.1371/journal.pone.0281721.

23. Guo, C., Zuo, Z., Feng, H., Jia, B. & Roskilly, T. “Review of recent advances of free-piston internal combustion engine linear generator”. *Applied Energy*. 2020; 269: 115084. DOI: https://doi.org/10.1016/j.apenergy.2020.115084.

24. Li, J., Zuo, Z., Liu, W., Jia, B., Feng, H., Wang, W., Smallbone, A. & Roskilly, A. P. “Generating performance of a tubular permanent magnet linear generator for application on free-piston engine generator prototype with wide-ranging operating parameters”. *Energy*. 2023; 278: 127851. DOI: https://doi.org/10.1016/j.energy.2023.127851.

25. Wang, J., Feng, H., Wei, Y., Ma, Y., Jia, B., Wei, S., Xu, L. & Lin, H. “Enhancing energy efficiency of free-piston engine generator through the controllable cycle method: Analysis of energy gain and consumption”. *Applied Energy*. 2025; 392: 126049. DOI: https://doi.org/10.1016/j.apenergy.2025.126049.

26. Liu, L., Guo, Y., Yin, W., Lei, G. & Zhu, J. “Design and optimization technologies of permanent magnet machines and drive systems based on digital twin model”. *Energies*. 2022; 15 (17): 6186. DOI: https://doi.org/10.3390/en15176186.

Received 25.07.2026
Received after revision 22.09.2026
Accepted 02.11.2026

DOI: https://doi.org/10.15276/aait.09.2026.40
УДК 004.9

Двоканальна синхронізація валів роторно-лопатевого двигуна з обмеженими електроприводами

Ушенко Юрій Олександрович[1)]
ORCID: https://orcid.org/0000-0003-1767-1882; y.ushenko@chnu.edu.ua. Scopus Author ID: 6701840218
Угрин Дмитро Ілліч[1)]
ORCID: https://orcid.org/0000-0003-4858-4511; d.ugryn@chnu.edu.ua. Scopus Author ID: 57163746300
Галін Юрій Олександрович[1)]
ORCID: https://orcid.org/0009-0006-9629-9896; halin.yurii@chnu.edu.ua
[1)] Чернівецький національний університет імені Юрія Федьковича, вул. Коцюбинського, 2. Чернівці, 58002, Україна

АНОТАЦІЯ

Електромагнітна синхронізація валів роторно-лопатевого двигуна внутрішнього згоряння потребує узгодження руху лопатей зі змінним газовим навантаженням за обмежених можливостей електроприводів. Метою статті є розроблення зв'язаної комп'ютерної моделі синхронізації валів, що враховує механічні й термодинамічні процеси та електричні обмеження синхронних приводів з постійними магнітами й векторним керуванням, орієнтованим за полем. Завдання полягають у формулюванні зв'язаних рівнянь валів, камер і приводів, розробленні двоканального алгоритму синхронізації, реалізації відтворюваного симулятора та визначенні впливу параметрів електроприводів, геометричного масштабу камер і витоку газу на стійкість руху. Модель поєднує механічну динаміку двох валів, газові процеси в робочих камерах з тепловиділенням і витоком через ущільнення та електроприводи з обмеженнями струму й напруги, індуктивністю й опором обмоток, пропорційно-інтегральним регулюванням струму, компенсацією протиелектрорушійної сили, механізмом захисту від інтегрального насичення, дискретним керуванням і скінченною смугою пропускання контуру струму. Модель перевірено за аналітичними розв'язками, енергетичними балансами, ідеальним циклом Отто та незалежними реалізаціями окремих блоків. Запропоновано двоканальний алгоритм з адаптивним регулюванням взаємного руху валів і корекцією положення бісектриси лопатей відносно корпусу, для якого встановлено локальні умови стійкості. Визначено вплив фізичного реверсу моменту та витоку газу на працездатність системи синхронізації. Симулятор дає змогу оцінювати придатність електромашин, налаштування регуляторів і геометричні параметри двигуна до створення експериментального стенда. У досліджених режимах алгоритм забезпечує мале усталене відхилення бісектриси та відновлення синхронізованого руху після пропуску запалювання, змін тепловиділення й навантаження. Працездатність алгоритму також підтверджено в серії чисельних випробувань із випадковими початковими умовами та варіаціями електричних параметрів досліджуваних приводів. Для обраного електропривода визначено діапазон допустимого об'єму камери зі згорянням, обмежений струмом за збільшення масштабу та витоком за його зменшення. Стійкість синхронізації визначається запасом моменту та швидкістю його формування; запаси за струмом і напругою є необхідними, але не достатніми умовами. Без згоряння привода достатньо для всіх досліджених об'ємів камер, тому цей режим придатний для початкових стендових випробувань. Отримані кількісні результати є модельними прогнозами та потребують експериментального підтвердження.

Ключові слова: комп'ютерне моделювання; роторно-лопатевий двигун; синхронізація валів; векторне керування; синхронний двигун; витік через ущільнення

ABOUT THE AUTHORS



Yurii O. Ushenko – Doctor of Physical-Mathematical Sciences, Head of Computer Science Department, Yuriy Fedkovych Chernivtsi National University, 2, Kotsyubynsky Str. Chernivtsi, 58002, Ukraine
ORCID: https://orcid.org/0000-0003-1767-1882; y.ushenko@chnu.edu.ua. Scopus Author ID: 6701840218
Research field: Information technologies and intelligence systems; digital signals and images processing

Ушенко Юрій Олександрович – доктор фізико-математичних наук, завідувач кафедри Комп'ютерних наук. Чернівецький національний університет ім. Ю. Федьковича, Коцюбинського, 2. Чернівці, 58002, Україна
Галузь досліджень: Інформаційні технології та інтелектуальні системи; обробка цифрових сигналів та зображень



Dmytro I. Uhryn – Doctor of Engineering Sciences, Professor, Computer Science Department. Yuriy Fedkovych Chernivtsi National University, 2, Kotsyubynsky Str. Chernivtsi, 58002, Ukraine
ORCID: https://orcid.org/0000-0003-4858-4511; d.ugryn@chnu.edu.ua. Scopus Author ID: 57163746300
***Research field*:** Information technologies for decision support; swarm intelligence systems; branch geoinformation systems

Угрин Дмитро Ілліч – доктор технічних наук, професор кафедри комп'ютерних наук, Чернівецький національний університет ім. Ю. Федьковича, Коцюбинського, 2. Чернівці, 58002, Україна
Галузь досліджень: Інформаційні технології для підтримки прийняття рішень; системи ройового інтелекту; галузеві геоінформаційні системи



Yurii O. Halin – PhD student, Computer Science Department. Yuriy Fedkovych Chernivtsi National University, 2, Kotsyubynsky Str. Chernivtsi, 58002,Ukraine
ORCID: https://orcid.org/0009-0006-9629-9896; halin.yurii@chnu.edu.ua
***Research field*:** Information technologies and intelligence systems

Галін Юрій Олександрович – аспірант кафедри Комп'ютерних наук. Чернівецький національний університет ім. Ю. Федьковича, Коцюбинського, 2. Чернівці, 58002,Україна
Галузь досліджень: Інформаційні технології та інтелектуальні системи